Electronic Supplementary Information

Optimized Ni(II)-doping in Co(III)-based Layered Double Hydroxides towards Electrochemical Oxygen Evolution Catalysis

Huiling Si , Yanhong Ma, Hang Zu and Jianbo Liang*
Department of Chemistry, Capital Normal University, Beijing, 100048,P. R. China.

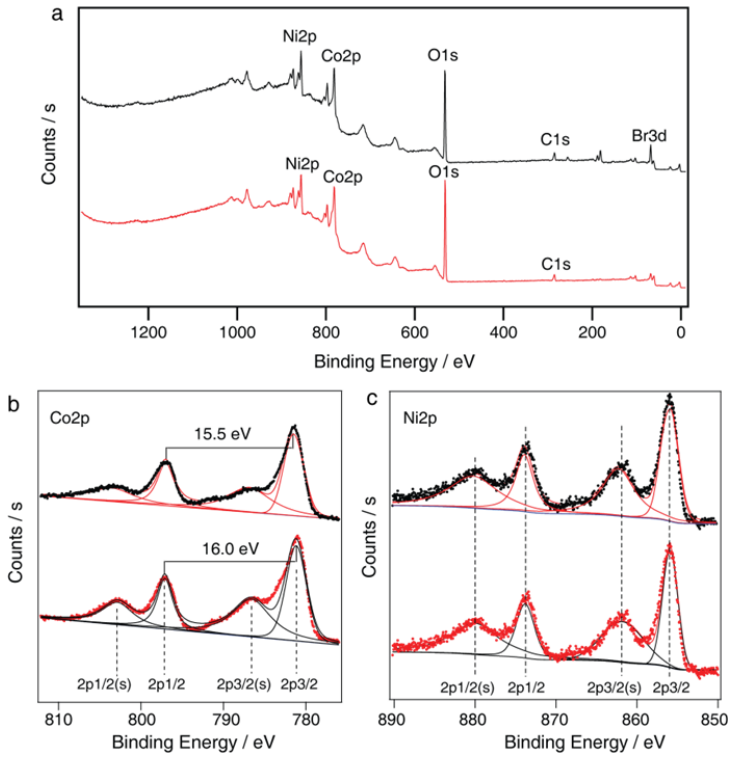

Figure S1. XPS spectra of the $Ni(II)_{0.2}Co(II)_{0.8}(OH)_2$ (red) and the $Ni(II)_{0.2}Co(II)_{0.47}Co(III)_{0.33}$ LDH sample (black): the survey spectra (a), the Co 2p profiles (b) and the Ni 2p profiles (c).

The Co 2p profile of $Ni(II)_{0.2}Co(II)_{0.8}(OH)_2$ presents two main peaks and corresponding satellite peaks: $2p_{3/2}$ (781.3 eV), $2p_{3/2}$(s) (785.9 eV), $2p_{1/2}$ (797.3 eV) and $2p_{1/2}$(s) (803.1 eV). The spin-orbit split value (16.0 eV) is very close to that of $Co(OH)_2$. The $2p_{3/2}$ satellite peak is prominent, which is a typical feature of Co(II) cations in high-spin state. For $Ni(II)_{0.2}Co(II)_{0.47}Co(III)_{0.33}$ LDH sample, the intensity of the $2p_{3/2}$ satellite peak is significantly reduced. The spin-orbit splitting value is reduced to 15.5 eV ($2p_{3/2}$: 781.4 eV, $2p_{1/2}$: 796.9 eV), which is close to that of CoOOH and Co_3O_4. Such spectral changes indicate the formation of trivalent Co cations. In contrast, the Ni 2p emissions for the two samples are nearly the same in both the location and the shape: $2p_{3/2}$ (855.9 eV), $2p_{3/2}$(s) (861.8 eV), $2p_{1/2}$ (873.6 eV) and $2p_{1/2}$(s) (879.9 eV), which indicates that Ni cations preserves the divalent state during the oxidation intercalation reaction.

See ref 21 in the main text for the detailed analysis.

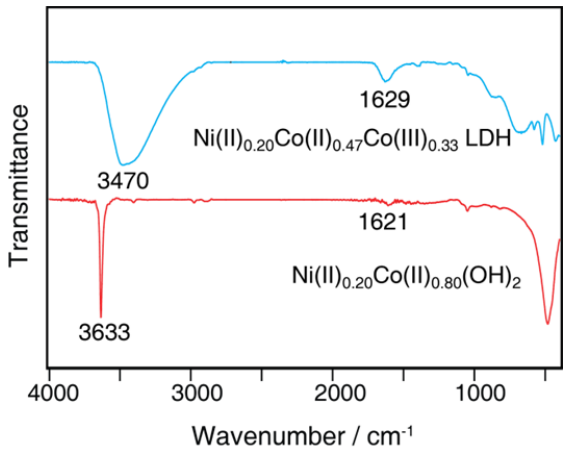

Figure S2. The FT-IR spectra of the $Ni(II)_{0.2}Co(II)_{0.8}(OH)_2$ (light blue) and the $Ni(II)_{0.2}Co(II)_{0.47}Co(III)_{0.33}$ LDH sample (red).

For $Ni(II)_{0.2}Co(II)_{0.8}(OH)_2$, the sharp peak centered at 3633 cm^{-1} is assigned as the stretching mode of OH groups. The sharp peak suggests the OH groups are free of hydrogen bonding. For the sample obtained after the oxidative intercalation, the spectrum presents a broad band centered at 3470 cm^{-1}, which are assigned as the stretching mode of OH groups associated with the hydrogen bonding. The changes of the OH stretching mode, both in the location and the peak shape, strongly support the formation of LDH structure.

See ref 21 in the maintext for the detailed analysis.

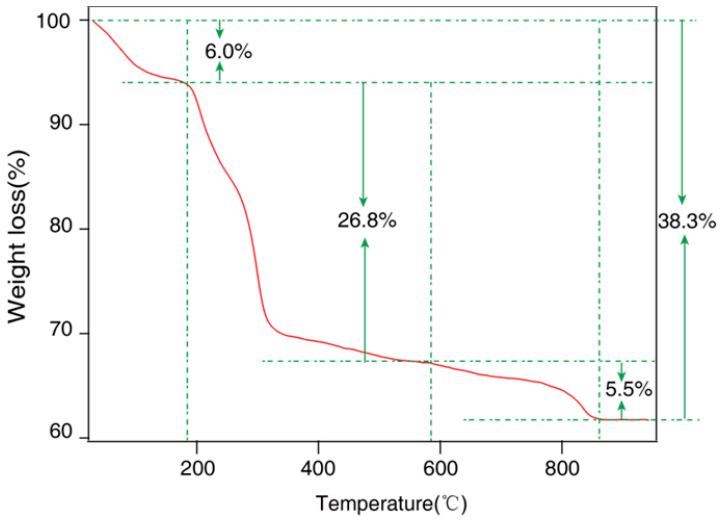

Figure S3. Thermogravimetric (TG) curve of the $Ni(II)_{0.2}Co(II)_{0.47}Co(III)_{0.33}$ LDH sample.

The first weight loss of 6.0% from room temperature to 190 ℃ is assigned as the loss of interlayer water molecules. The second weight loss from 190 to 580 ℃ (26.8%) is aroused from the dehydroxylation of the host layers and the release of interlayer species from the solid. The product transforms into Co_3O_4 when heated to this temperature. The third weight loss above 600 ℃ is the transformation of Co_3O_4 to a CoO by releasing oxygen from the solid.

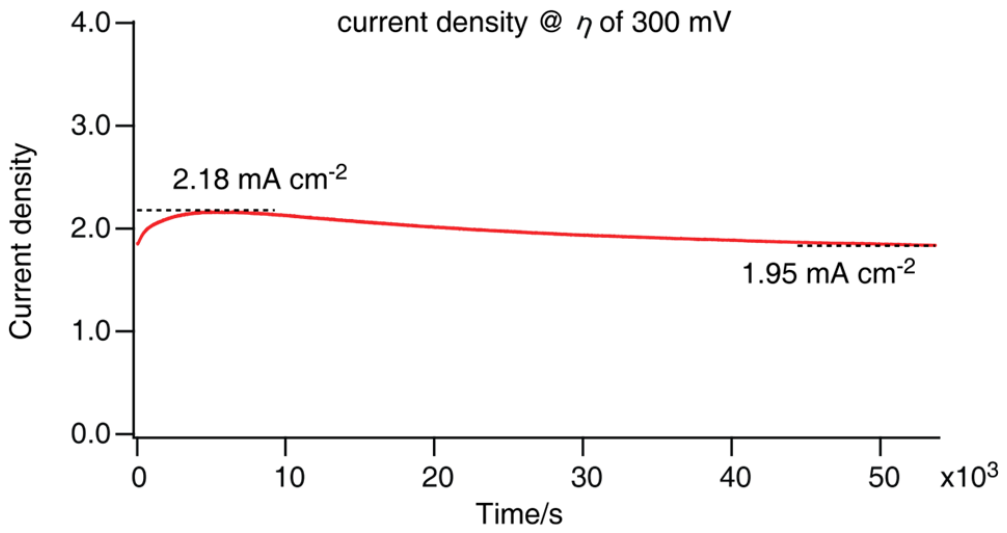

Figure S4. The stability of the $Ni(II)_{0.2}Co(II)_{0.47}Co(III)_{0.33}$ LDH sample.

The stability of the sample is measured by a potentiostatic method at overpotential of 300 mV. An increase of the current density at the initial stage may be resulted from the activation of the catalyst. The current density reaches 2.18 $mA{\cdot}cm^{-2}$ and is decreased to 1.95 $mA{\cdot}cm^{-2}$ after the catalyst is working for 50000 s. The current density keeps above 90% of the highest value during the test, showing the good stability of the catalyst.

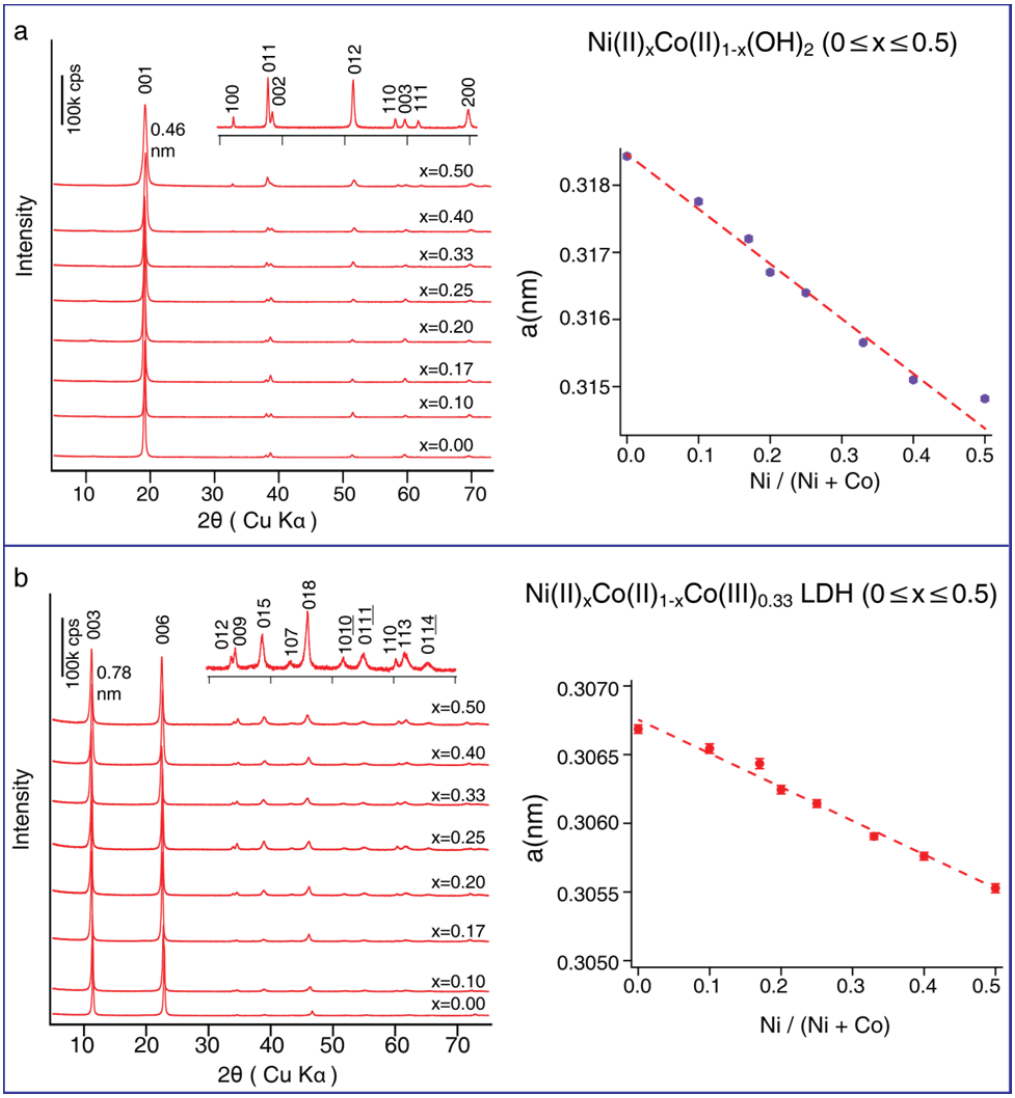

Figure S5. (a) XRD patterns of the $Ni(II)_xCo(II)_{1-x}(OH)_2$ ($0 \le x \le 0.5$) samples and the in-plane cell parameter of *a* plotted as a function of the fraction of Ni(II); (b) XRD patterns of the $Ni(II)_xCo(II)_{0.67-x}Co(III)_{0.33}$ LDH samples derived from the oxidative intercalation reaction and the plot of the in-plane cell parameter of *a* vs. the fraction of Ni(II).

Both the $Ni(II)_xCo(II)_{1-x}(OH)_2$ and the $Ni(II)_xCo(II)_{0.67-x}Co(III)_{0.33}$ LDH samples are phase-pure. The indexed diffraction peaks are shown by the sample with x=0.50. The sharp and intense basal peaks of samples show the high crystallinity of these samples. In the plot of the cell parameter of *a* (the in-plane cell parameter) vs. the fraction of Ni(II), the linear fitting indicates a uniform distribution of Ni(II) cations in the host layer.

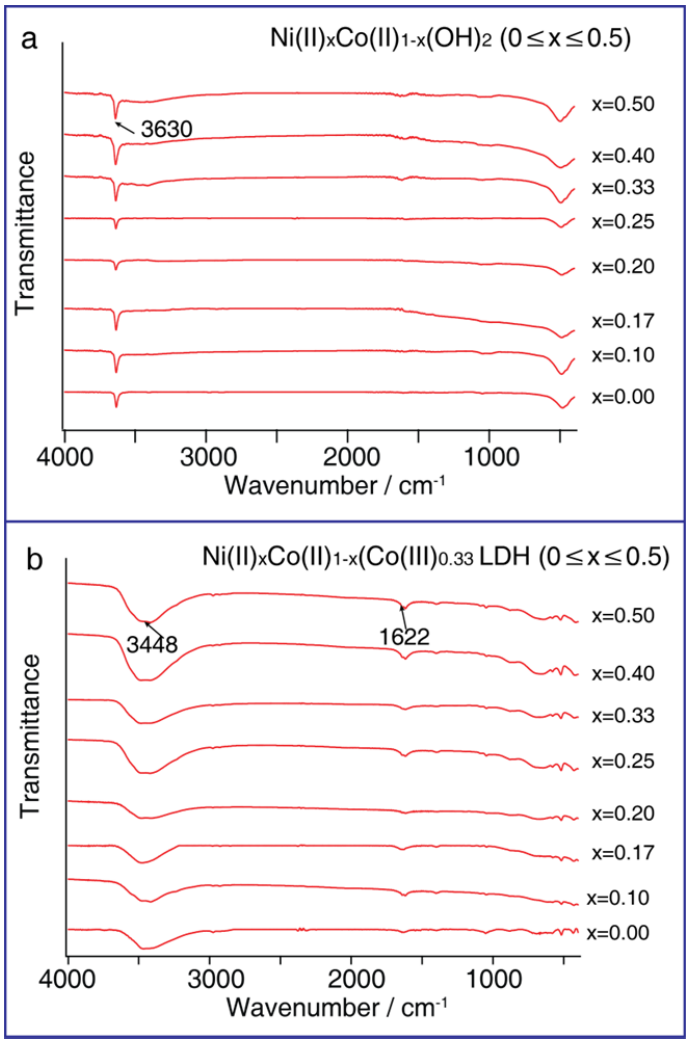

Figure S6. FT-IR spectra of the $Ni(II)_xCo(II)_{1-x}(OH)_2$ (a) and the $Ni(II)_xCo(II)_{0.67-x}Co(III)_{0.33}$ LDH ($0 \le x \le 0.5$) samples (b).

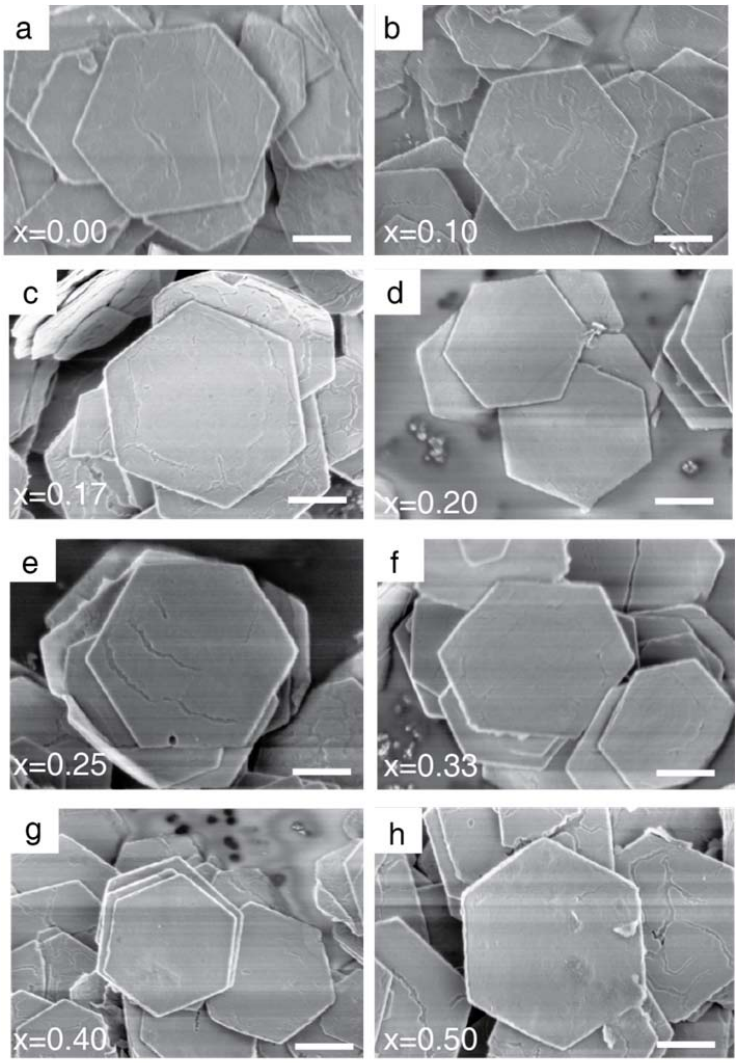

Figure S7. SEM images of the $Ni(II)_xCo(II)_{0.67-x}Co(III)_{0.33}$ LDH samples ($0 \le x \le 0.5$).The scale bar is 2 μm.

The SEM images show that the $Ni(II)_xCo(II)_{0.67-x}Co(III)_{0.33}$ LDH samples consist of well-developed hexagonal microplatelets. The edge length of the microplatelets is ringed in 1-4 μm, and the thickness is of several tens of nanometers. The same morphology and very close particle size manifest the very close physical surface area of these samples.

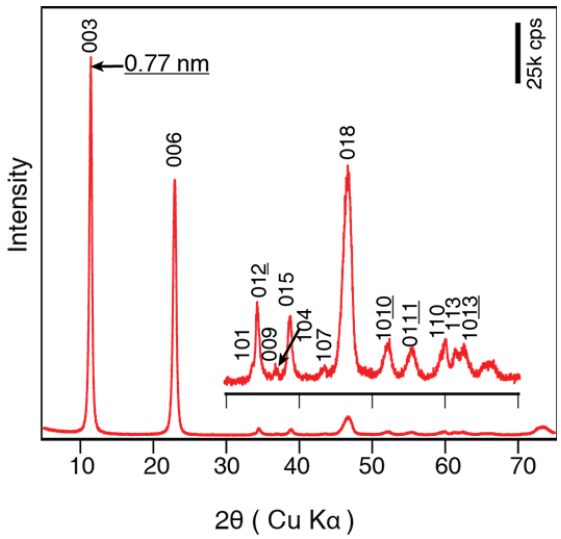

Figure S8. The indexed XRD pattern of the Ni(II)-Fe(III) LDH sample synthesized by the hydrothermal method. The basal spacing of 0.77 nm is consistent with those LDH samples intercalated by CO_3^{2-} ions.

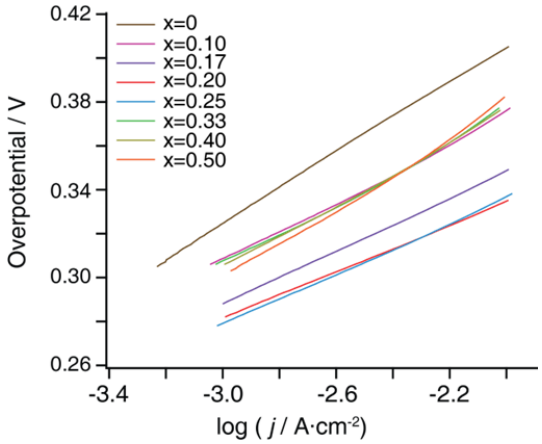

Figure S9. The Tafel slopes of the $Ni(II)_xCo(II)_{0.67-x}Co(III)_{0.33}$ LDH samples ($0 \le x \le 0.5$). The Tafel slope is calculated by the current density data ranged in 1–10 $mA \cdot cm^{-2}$.

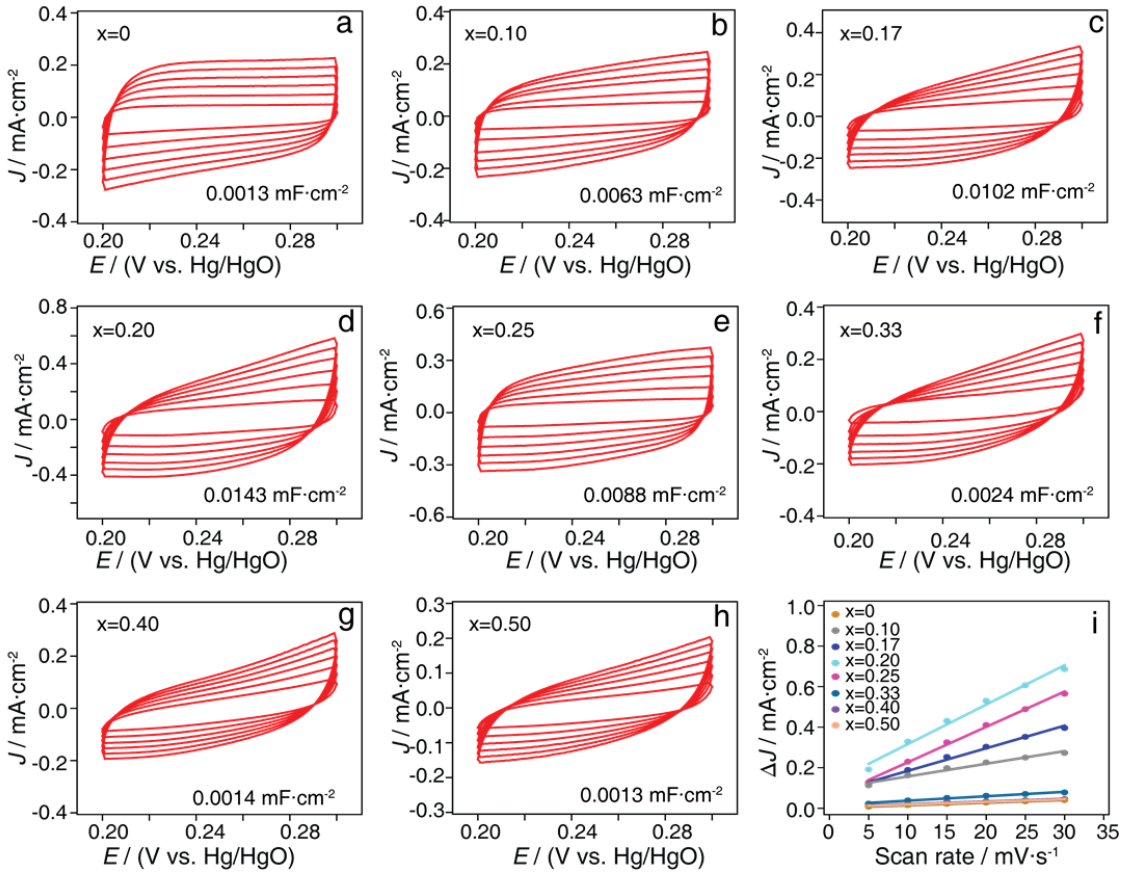

Figure S10. Double-layer capacitance (C_{dl}) measurements of the $Ni(II)_xCo(II)_{0.67-x}Co(III)_{0.33}$ LDH samples ($0 \le x \le 0.5$). (a) to (h) are the cyclic voltammograms of these LDH samples at varied scan rates (5, 10, 15, 20, 25, 30 $mV \cdot s^{-1}$). (i) is the plot of the ΔJ vs. the scan rate. $\Delta J = |J_a - J_c|$, in which J_a and J_c are the current densities measured at 0.25 V in the anodic and cathodic procedure, respectively.

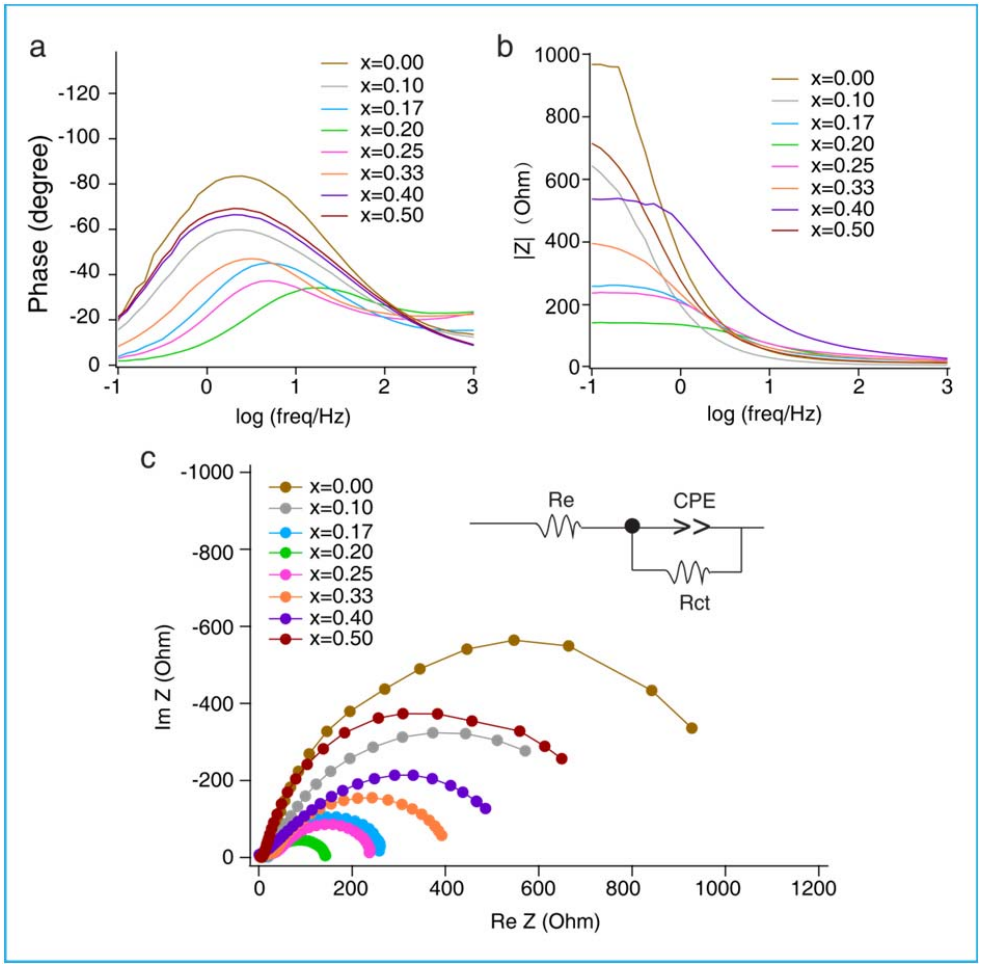

Figure S11. The Bode plot (a and b) and the Nyquist plot (c) of the $Ni(II)_xCo(II)_{0.67-x}Co(III)_{0.33}$ LDH samples ($0 \leq x \leq 0.5$) at 1.65 V (vs. RHE) in 1 M KOH. These LDH samples show different the impedance as a function of the fraction of Ni(II). For the LDH sample with x=0.20, the maximum of the phase angle locates at a higher frequency portion, which suggests a faster charge-transfer behavior. In the Nyquist plot, this sample also presents the lowest charge-transfer resistance. The EIS data is fitted by an equivalent circuit model is shown in figure c.

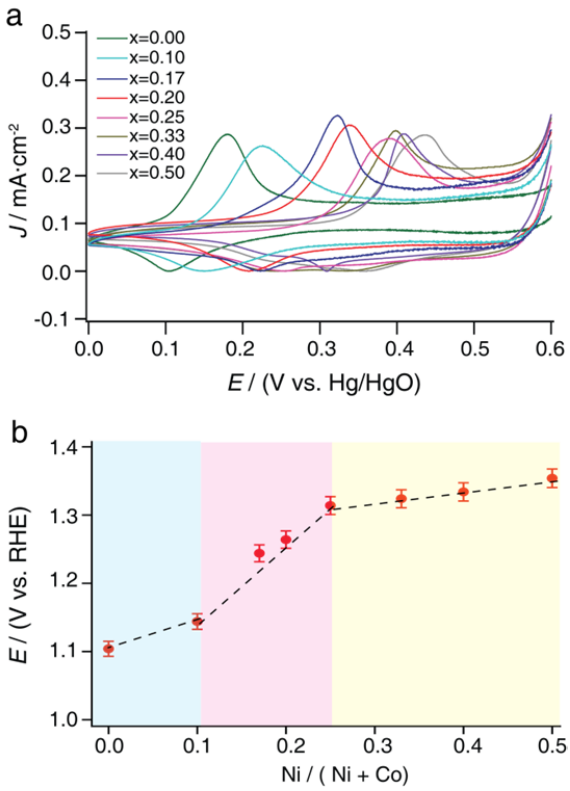

Figure S12. CV curves (a) of the $Ni(II)_xCo(II)_{0.67-x}Co(III)_{0.33}$ LDH samples ($0 \le x \le 0.5$) and a plot of the central position of the oxidative wave vs. the fraction of Ni(II) (b). In the CV curves, the shift of the oxidative wave is not uniform. As shown in (b), the shift is prominent for samples with $0.10 \le x \le 0.25$.

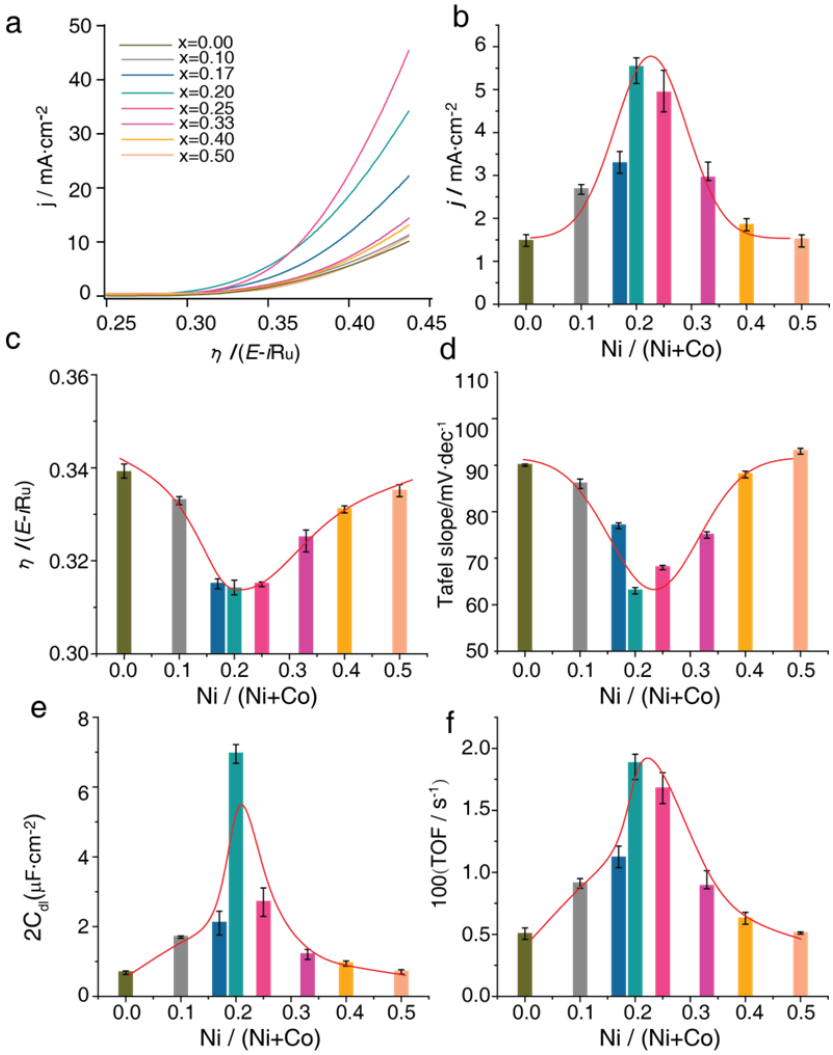

Figure S13. Evaluation of OER activity of the $Ni(II)_xCo(II)_{1-x}(OH)_2$ samples ($0 \le x \le 0.5$) in 1M KOH: the LSV curves at scan rate of 5 $mV \cdot s^{-1}$ (a), the current densities at η of 350 mV (b), the η determined at current density of 10 $mA \cdot cm^{-2}$ (c), the Tafel slope (d); the ECSA values .f) is the TOF calculated from η of 350mV.

The figures show that the OER activities of the $Ni(II)_xCo(II)_{1-x}(OH)_2$ samples present a volcano-like trend vs. the fraction of Ni dopant. This feature is similar to that in the $Ni(II)_xCo(II)_{0.67-x}Co(III)_{0.33}$ LDH samples while the former set of samples show significantly lower activity. The peak performance is observed at the sample of $Ni(II)_{0.20}Co(II)_{0.80}(OH)_2$. Ni(II)-doping leads to 4-fold enhancement of the OER activity, which is calculatedfrom the TOF of the $Ni(II)_{0.20}Co(II)_{0.80}(OH)_2$ and the $Co(II)(OH)_2$.

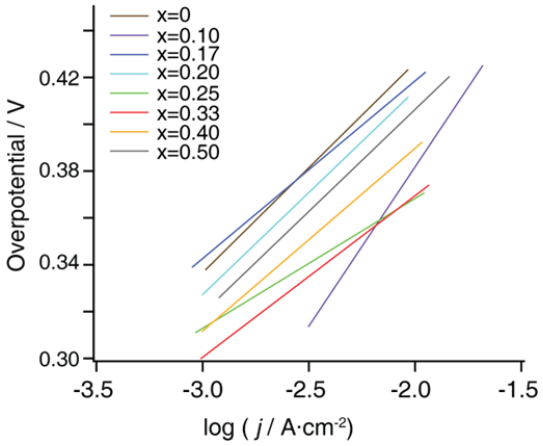

Figure S14. The Tafel slopes of the $Ni(II)_xCo(II)_{1-x}(OH)_2$ samples ($0 \le x \le 0.5$). The Tafel slopes is calculated from the current density data ranged in 1–10 $mA \cdot cm^{-2}$.

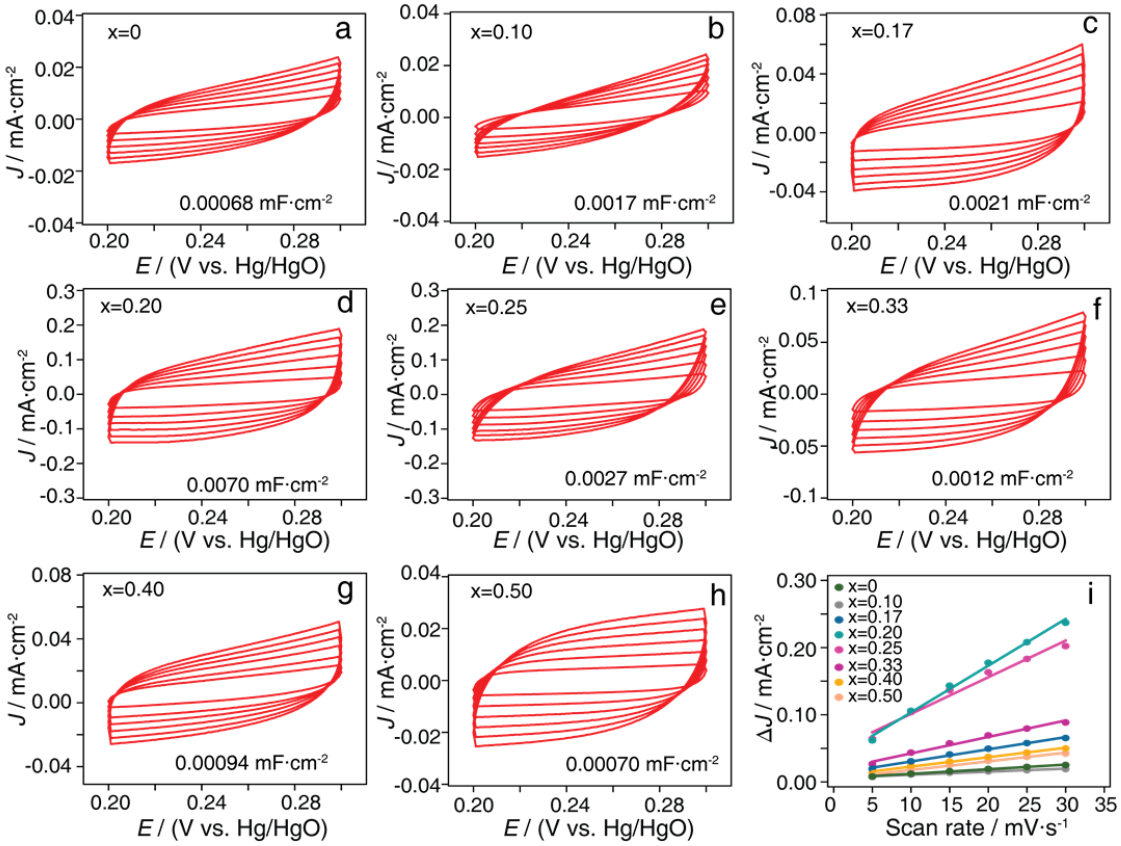

Figure S15. Double-layer capacitance (C_{dl}) measurements of the $Ni(II)_xCo(II)_{1-x}(OH)_2$ samples ($0 \le x \le 0.5$). (a) to (h) are the cyclic voltammograms of these samples at varied scan rates (5, 10, 15, 20, 25, 30 $mV \cdot s^{-1}$) ; (i) is the plot of the ΔJ vs. the scan rate. $\Delta J = |J_a - J_c|$, in which J_a and J_c are the current densities measured at 0.25 V in the anodic and cathodic procedure, respectively.

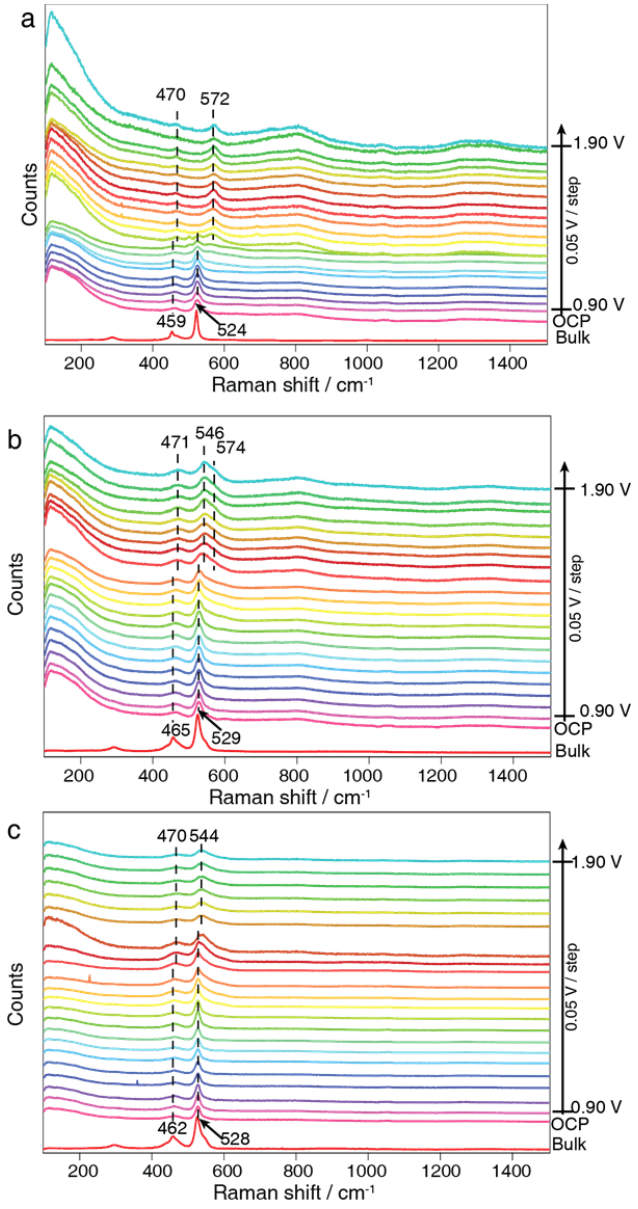

Figure S16. The full Raman spectra of the three $Ni(II)_xCo(II)_{0.67-x}Co(III)_{0.33}$ LDH samples : x=0.00 (a), x=0.20 (b) and x=0.33 (c). The signal of the oxygen radicals is often observed in 800-1200 cm^{-1}. Such signals are not clearly observed in our studies. The low yield of these species resulted from the fast kinetics may make it difficult to be detected.